Provided for non-commercial research and education use.
Not for reproduction, distribution or commercial use.

This article was published in an Elsevier journal. The attached copy is furnished to the author for non-commercial research and education use, including for instruction at the author's institution, sharing with colleagues and providing to institution administration.

Other uses, including reproduction and distribution, or selling or licensing copies, or posting to personal, institutional or third party websites are prohibited.

In most cases authors are permitted to post their version of the article (e.g. in Word or Tex form) to their personal website or institutional repository. Authors requiring further information regarding Elsevier's archiving and manuscript policies are encouraged to visit:

http://www.elsevier.com/copyright

Author's personal copy

ELSEVIER

Available online at www.sciencedirect.com
ScienceDirect

Thin Solid Films 516 (2008) 3105–3111

thin solid films
www.elsevier.com/locate/tsf

Fabrication of transparent conducting amorphous Zn–Sn–In–O thin films by direct current magnetron sputtering

Cleva W. Ow-Yang [a,*], Hyo-young Yeom [b], David C. Paine [b]

[a] *Sabanci University, Faculty of Engineering and Natural Sciences, Orhanli, Tuzla, 34956 Istanbul, Turkey*
[b] *Brown University, Division of Engineering, Box D, Providence, Rhode Island 02912, USA*

Received 2 January 2007; received in revised form 2 July 2007; accepted 24 July 2007
Available online 10 August 2007

Abstract

Amorphous ZnO–SnO_2–In_2O_3 films were grown by direct current magnetron sputtering from vacuum hot pressed ceramic oxide targets of Zn:In:Sn cation ratios 1:2:1 and 1:2:1.5 onto glass substrates. X-ray diffraction analysis showed that the microstructure remained amorphous during annealing at 200 °C for up to 5 hours. By monitoring the electrical resistivity, oxygen content and substrate temperature were optimized during deposition. The optimal films were characterized by Hall Effect, work function and optical spectroscopy measurements. Films of 1:2:1 composition showed the lowest resistivity (7.6×10^{-4} Ω-cm), when deposited onto substrates preheated to 300 °C. Transmissivity of all films exceeded 80% in the visible spectral region. The energy gap was 3.52–3.74 eV, and the work function ranged 5.08–5.22 eV, suitable for cathode applications in organic light emitting diodes. Overall, the film characteristics were comparable or superior to those of amorphous tin-doped indium oxide and zinc-doped indium oxide films and may serve as viable, lower-cost alternatives.
© 2007 Elsevier B.V. All rights reserved.

Keywords: Transparent conducting oxide; Indium tin oxide; Amorphous semiconductor; physical vapor deposition; Photoelectron spectroscopy; Work function; Optical properties; Hall Effect

1. Introduction

Transparent conductive oxide (TCO) thin films enable a wide variety of applications that require optical access in the visible region through the electrode materials. In the flat panel display (FPD) industry, films of two In-rich compositions are predominantly used-indium oxide doped with tin (ITO; In_2O_3–10 wt.% SnO_2) and, increasingly, doped with zinc (IZO; In_2O_3–10 wt.% ZnO) to stabilize the amorphous microstructure of room temperature, as deposited films. Such films show metal-like electrical resistivity, $1–2 \times 10^{-4}$ Ω-cm and $3–6 \times 10^{-4}$ Ω-cm respectively, and transmissivity of 80–90% of visible light. Despite a slightly higher resistivity, *a*-IZO films are more attractive for FPD applications that require a faster, isotropic wet etch rate, enabling the transfer of finer line-width patterns.

The high cost and relative scarcity of indium encourages the development of lower-cost alternatives to *a*-ITO and *a*-IZO, motivating extensive investigation for candidate replacement TCO materials such as ZnO [1]. However, the performance of indium-based TCO materials and their well established processing parameters and wide processing window, combined with an excellent chemical and physical stability in the thin film form, suggests that adoption of new materials may meet resistance. In particular, materials that preserve the processing and service performance of amorphous IZO are of great interest. One possibility is the use of ternary oxides of ZnO–In_2O_3–SnO_2 (ZITO) system, which retains the highly stable amorphous structure of *a*–IZO but displaces as much indium oxide as possible by incorporation of ZnO and SnO_2.

In the crystalline state, ZnO has a very low solid solubility in In_2O_3 (<1 wt.%) due to the requirement that divalent zinc assumes a tetrahedral coordination with oxygen while trivalent In requires six-fold oxygen coordination. In the amorphous state, the coordination polyhedra would be preserved, but much higher concentrations of ZnO in In_2O_3 have been reported [2]. It appears that the presence of the ZnO stabilizes the amorphous structure, by inhibiting the ability of the indium octahedra to

* Corresponding author. Tel.: +90 216 483 9592; fax: +90 216 483 9550.
E-mail address: cleva@sabanciuniv.edu (C.W. Ow-Yang).

0040-6090/$ - see front matter © 2007 Elsevier B.V. All rights reserved.
doi:10.1016/j.tsf.2007.07.205

Author's personal copy

relax and rotate into the complex bixbyite structure of the thermodynamically stable crystalline phase. When the material did recrystallize at high temperatures (*i.e.*, at 500 °C annealed in air), it formed a complex, interleaved, layered structure of alternating layers of InO_6 and ZnO_4 polyhedral units [3]. ITO, by contrast, begins to crystallize at significant rates at temperatures as low as 120 °C [4].

Previous work on ZITO systems has focused on targets in which co-substitution of SnO_2 and ZnO in In_2O_3 was demonstrated to increase the bulk solid solubility of both components up to ~20 wt.% for each [5]. Thin films sputtered directly from such targets tended to have poor crystallinity in the as-deposited state, attributable to structural frustration while attempting to accommodate the preferred tetrahedral coordination of Zn^{2+} together with the octahedral coordination of In^{3+} and of Sn^{4+}. Such films offer an enormous technological advantage—a highly isotropic wet-etch uniformity would enable higher resolution lithographic patterning.

When sputtering a multi-cation-containing target, control over the film composition produced has been limited. In particular, different oxidation potentials among the cations could give rise to films with a stoichiometry differing from that of the target [6], while surface adsorption-limiting kinetics could also enable the formation of metastable phases. To compare amorphous films of different composition, the ratio of the relative amounts of different cation species was used. Accordingly, electrical and optical properties have been reported to be tunable via the film composition, when prepared by pulsed laser deposition [6] and radio frequency magnetron sputtering [7]. The best reported values for resistivity ranged from $3–8 \times 10^{-4}$ Ω-cm, from ~2.9–3.65 eV for the absorption edge and a work function of ~4.9 eV. Films closer to thermodynamic equilibrium conditions were also produced by metal organic chemical vapor deposition, and their optical properties offered an even wider window of visible light transmission than ITO [8].

To complement the existing literature, we are reporting the deposition of ZITO from ceramic targets using direct current (dc) magnetron sputtering [9]—the manufacturing technique of choice for IZO and ITO in the display industry, due to its large area uniformity. In this paper we present an investigation of the properties of thin films grown by dc magnetron sputtering from two hot-pressed ceramic oxide targets of ZITO, one containing equal amounts of Zn and Sn (1:2:1 cation ratio) and the second being a Sn-rich composition (1:2:1.5 cation ratio). O_2 partial pressure was varied to identify the optimal film deposition conditions [10]. Then, using the optimized deposition conditions, ZITO films were deposited onto glass substrates both at room temperature and pre-heated to 300 °C. To evaluate the performance of ZITO films compared to ITO and IZO, Hall Effect and work function measurement were used to characterize the electrical properties, while the optical properties were characterized by ultraviolet (UV)-visible-near-infrared (IR) spectroscopy.

2. Experimental details

Sputter targets were vacuum hot pressed at 900 °C in Ar from ball-milled ZnO and In_2O_3 powders. To achieve stoichiometric isovalent substitution of In, a target was prepared with a nominal cation ratio of 1:2:1, 10.3 wt.% ZnO and 19.1 wt.% SnO_2. One with excess Sn was prepared with a composition of 9.4 wt.% ZnO_2 and 26.6 wt.% SnO_2, for a cation ratio of 1:2:1.5. Fig. 1 shows the XRD patterns of the target phase compositions, both of which contain a mixture of bixbyite indium oxide, tin oxide, and ternary Zn_2SnO_4 and $In_4Sn_3O_{12}$ phases.

ZITO thin films were deposited onto Corning 0211 glass substrates, with the substrates either unheated or preheated to 300 °C, from each of the two multiphase targets by dc magnetron sputter deposition at a rate of 0.1 nm/s. A total system pressure of 4 Pa and a sputter power of 0.22 W/cm^2 at 280 V were used. The resistivity of the as-deposited material was optimized by adjusting the reactive oxygen content $O_2/(O_2+Ar)$ over a range of 0–10 vol.% in the sputter gas during deposition of a series of 100-nm thick films. A multi-beam optical stress sensor technique [10] was used to calculate $\Delta V/V$ from measured stress-induced structural changes. The optimization results are shown in Fig. 2. For further electrical and optical characterization, a set of films of thickness 43 nm, 93 nm, 138 nm, and 189 nm (±.5 nm) was produced using the optimum conditions for the 1:2:1 ZITO target, *i.e.* with the substrate preheated to 300 °C and a pure (0 vol.% O_2) Ar sputter gas.

Samples for Hall Effect measurements were patterned lithographically using the lift-off technique to obtain the necessary geometry of Hall spiders. The films were annealed at 200 °C in air, during which Hall Effect measurements were performed *in-*

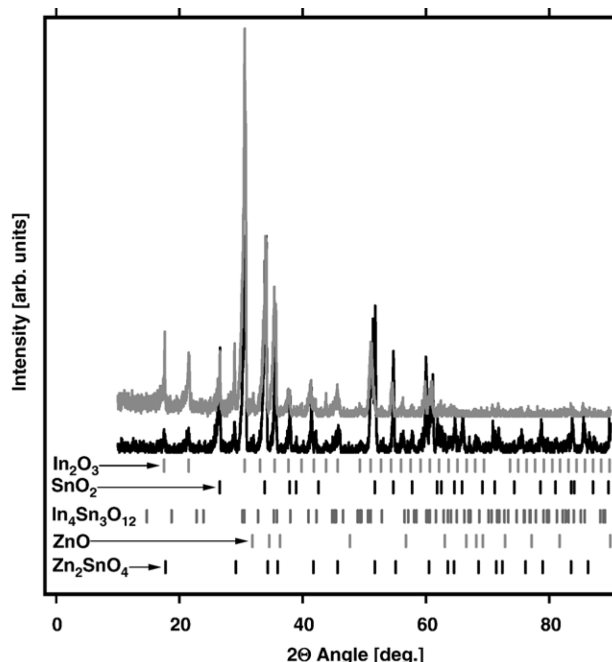

Fig. 1. X-ray diffraction patterns from the two ZITO targets used in this work, of cation ratios 1:2:1 and 1:2:1.5. ZITO 1:2:1 target (solid black line) has a composition of 10.3 wt.% ZnO + 19.1 wt.% SnO_2, balanced with In_2O_3, while the ZITO 1:2:1.5 target (dotted gray line) has a composition of 9.4 wt.% ZnO + 26.2 wt.% SnO_2, balanced with In_2O_3. Both targets contain a mixture phases of as shown in comparison with the standard International Center for Diffraction Data database files for In_2O_3 (note the characteristic {222} peak at ~33°), $ZnSnO_3$, ZnO, $In_4Sn_3O_{12}$, and for SnO_2 [31].

Author's personal copy

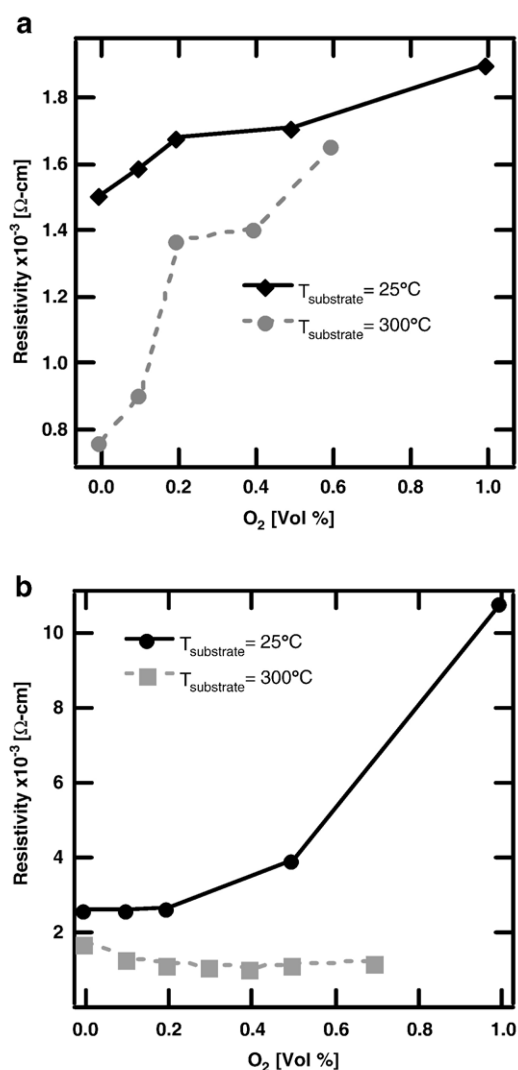

Fig. 2. Optimization of resistivity by varying the reactive O_2 content in the sputter gas for 100-nm thick films grown from target compositions (a) ZITO 1:2:1 and (b) ZITO 1:2:1.5.

situ to monitor the effect of oxygen incorporation extent on electronic conductivity, carrier concentration, and mobility. Work function measurements were carried out using photoelectron spectroscopy in air (AC-2, Riken Keiki), according to the sample preparation and measurement procedures described by Sato et al. [11]. UV-visible-near-IR spectroscopy (UV-3150, Shimadzu) was performed to obtain the transmittance and reflectance spectra and determine the energy gap.

3. Results and discussion

X-ray diffraction (XRD) analysis with monochromatic Cu–K_α (λ=0.154 nm) radiation revealed the broad, diffuse peak characteristic of amorphous materials for the as-deposited films on both unheated and 300 °C-heated substrates. The films remained amorphous after prolonged (>300 min) heating at 200 °C in air. Such metastable behavior is similar to that observed in amorphous films of In_2O_3 doped with 10 wt.% ZnO, which are remarkably stable at elevated temperatures [3], which can be attributed to crystal structure frustration arising from accommodating different metal oxide coordination structures. In_2O_3 tends to crystallize in a bixbyite crystal structure consisting of MO_6 coordination units, while ZnO prefers the wurtzite structure with MO_4 coordination units. In the case of the ZITO films, the higher concentrations of Zn cations would similarly stabilize the amorphous structure and increase the activation energy demanded for an ordering transformation to occur. However, the higher concentrations of Sn should not contribute significantly to crystal structure frustration, since SnO_2, although crystallizing in a rutile crystal structure, also prefers MO_6 coordination units.

Films with the nominal target cation ratio 1:2:1 were also characterized in a field-emission scanning electron microscope by quantitative energy-dispersive X-ray spectroscopy. The composition of the amorphous films was revealed to have a cation ratio closer to (2.2):(2.5):1.

Electrical properties were optimized by incorporating increasing amounts of oxygen into the films during post-deposition annealing at 200 °C in air. Fig. 2 shows the evolution of electrical resistivity with increasing oxygen vol.%, for films grown from both targets. When deposited in an oxygen-free ambient, the best properties were obtained for as-sputtered films from the 1:2:1 target. According to the measured resistivity, carrier concentration, and mobility values listed in Table 1, the film grown on a 300 °C pre-heated substrate performing half an order of magnitude better than the unheated substrate. In contrast, the nominal 1:2:1.5 film deposited onto a 300 °C substrate required the incorporation of 0.4 vol.% of oxygen, in order to achieve a minimum in resistivity. The difference in required oxygen content for achieving an optimum resistivity between the two films indicated that different mechanisms of electrical conductivity were operating, as also observed when comparing studies of other In_2O_3-based films (see Fig. 3). The films for which resistivity was optimized by oxygen incorporation were *a*-$In_2O_{3-\delta}$, *a*-ITO, *c*-ITO, and 1:2:1.5 ZITO, whereas resistivity increased steadily in *a*-IZO and in 1:2:1 *a*-ZITO.

To understand the observations in Figs. 2 and 3, the sources of electrical charge carriers in the films should be considered. Nominally pure, *i.e.* unintentionally doped, In_2O_3 is known to grow with a high deficiency of oxygen [12], giving rise to doubly charged oxygen vacancy defects that determine the highly degenerate, *n*-type semiconductor behavior. Even with Sn doping, when singly charged $Sn_{In}^{\bullet}$ may form in the crystalline material, experimental evidence [13] indicates that not all of the Sn dopant ions are electrically active. In the case of

Table 1
Results of Hall Effect measurements on dc magnetron-sputtered ZITO films: comparing target composition and substrate temperature effects

Target composition cation ratio	Substrate temperature [°C]	Resistivity [$\times 10^{-3}$ Ω-cm]	Hall mobility [cm^2/V-s]	Carrier concentration [$\times 10^{20}$ cm^{-3}]
1:2:1	RT	1.50	30.23	1.27
1:2:1	300	0.77	32	1.87
1:2:1.5	RT	2.58	26.87	0.90
1:2:1.5	300	1.03	40.35	1.50

Author's personal copy

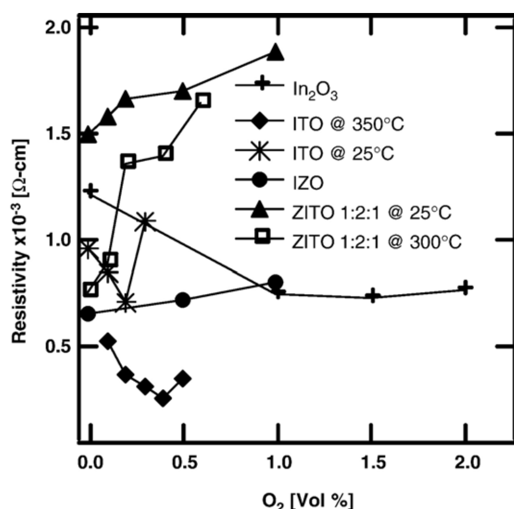

Fig. 3. Comparison of resistivity optimization for the ZITO 1:2:1 films against other In_2O_3-based films[14]-In_2O_3, Sn:In_2O_3, $In_2Zn_{0.38}O_{3.38}$-deposited onto both unheated and pre-heated substrates.

amorphous ITO films, the carrier concentration was observed to be independent of Sn dopant concentration, suggesting that it is not activated in the disordered structure [6]. But regardless of crystallinity, the oxygen vacancies would be the prevailing contributor of electrical charge carriers in In_2O_3 and ITO films, and the observations in Fig. 3 are consistent with reported behavior in the literature [14], in which the incorporation of oxide ions (O^{2-}) would eliminate oxygen vacancies. The available mobile electronic charge concentration would decrease, but the increase in charge carrier Hall mobility would compensate, due to the removal of scatter centers. The electrical conductivity would thus increase with increasing oxygen content up to an optimal value. Above that value, the excess oxygen ions could form associated complexes, such as with Sn ions, thereby decreasing mobility by increasing the scatter center population, and arresting the increase in mobile charge carriers.

However, the existing models do not explain the evolution of resistivity with oxidation in the case of films sputtered from the 1:2:1 target. These films should have contained a high density of oxygen vacancy defects and therefore should have readily incorporated oxygen to allow optimization of electrical properties via the elimination of oxygen defects. We should have observed an optimized film containing some non-zero volume percentage of oxygen incorporation, because the charge carrier concentration would decrease due to elimination of a source of electronic charge carriers, but the mobility would increase due to the elimination of scatter centers. To elucidate the different mechanisms, we investigated the changes in electrical resistivity, charge carrier concentration, and charge mobility with increasing oxygen incorporation (Fig. 4).

The most dramatic changes occurred during the initial 15 min of annealing, which was consistent with a volume expansion of 5%, followed by more gradual expansion of ~1.25% over the next 155 min. This trend was reflected by an accompanying increase in the charge carrier density and mobility and decrease in resistivity, during the transient period. The subsequent drop in carrier concentration was accompanied by a more gradual increase in mobility and an increase in resistivity until reaching steady state at 170 min of annealing. One feature that appears contradictory in this plot is where both the charge carrier concentration and mobility increased simultaneously during the initial stage of oxygen incorporation. According to existing models of electronic conductivity for In_2O_3-based films [14], we would have expected the carrier concentration to decrease upon oxidation continuously, while the mobility increase was consistent with observations of structural relaxation during this time period.

One possible explanation would be that the ZITO films grown by sputtering from the 1:2:1 cation ratio target were highly oxygen deficient, since pure argon gas was used in the deposition chamber. Assuming that the Sn dopant, even if only slightly in excess, would not be activated in the *a*-ZITO film, as was the case for *a*-ITO films, then oxygen would only be incorporated into oxygen vacancy defects and would not participate in defect complexes. Also, recognizing that the sputter deposition produced optimal films in an *oxygen-free* sputter gas, the as-deposited films could contain reduced Zn cations in the Zn^{1+} state. These defects would be oxidized and release an electron during the initial incorporation of ionized oxygen anions into the film. Such a process would contribute to an increase in the carrier concentration, with minimal impact on the charge carrier Hall mobility.

By first pre-heating the glass substrates to 300 °C in vacuum, films were produced with a resistivity improved by roughly half an order of magnitude, as shown in Fig. 2a, due to increases in both charge carrier concentration and Hall mobility. The higher temperature substrates provided the adsorbed atoms with more energy to diffuse along the surface to seek an energetically favorable position. Although the additional thermal energy could have aided assembling into some higher degree of short-range order, the complicated structural requirements of the

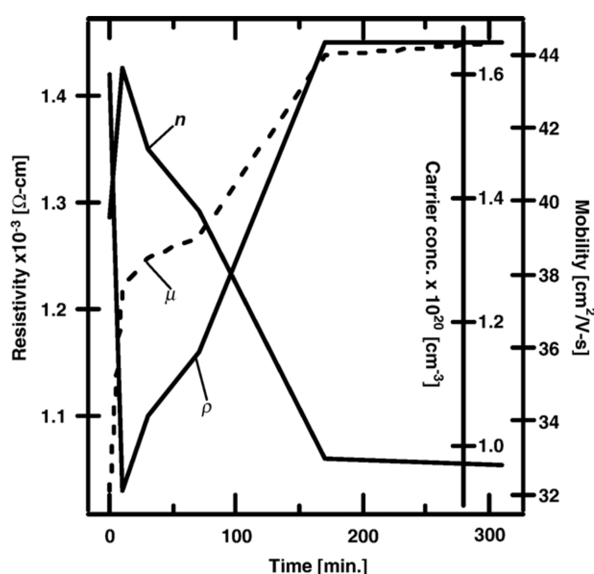

Fig. 4. Evolution in resistivity (solid black line), carrier concentration (dotted gray line), and mobility (dashed black line) with extent of oxygen incorporation by annealing a ZITO film sputter deposited from the 1:2:1 cation ratio target in air at 200 °C.

Author's personal copy

ZITO films still stabilized the amorphous indium oxide structure, as was reported by Yaglioglu and co-workers for amorphous indium zinc oxide [15]. To clarify this point, we would need to compare the radial distribution function between films deposited onto unheated and heated substrates. Nonetheless, the improvement on electronic properties was clear in comparison with the unheated substrates.

Fig. 2b shows the optimization of resistivity for films sputtered from the nominally 1:2:1.5 target, *i.e.*, the one containing excess Sn. Although deposition on in an O_2-free ambient produced films with the lowest resistivity on unheated substrates, an even lower resistivity was obtained on a 300 °C-heated substrate by depositing with 0.4 vol.% O_2 in the ambient gas, similar to behavior observed in as-deposited, oxygen-deficient ITO films. Finally, the excess Sn dopant in these films provided extra ionized impurity scattering centers, lowering the mobility and hence increasing the resistivity, compared to the films with more equal amounts of Zn to Sn.

As an alternative TCO to ITO or IZO, the electrical charge carrying properties of the ZITO films compared reasonably well. The lowest electrical *resistivity* of 7.6×10^{-4} Ω-cm is slightly higher than that of *a*-IZO, $3–6\times10^{-4}$ Ω-cm [16]. This increase could be attributed to the lower charge carrier *Hall mobility* (32 vs. 52 cm^2/V-s) arising from the additional substitutional Sn scatterers. For *a*-ITO, the lowest resistance is 7×10^{-4} Ω-cm [17].

To measure the surface work function, the films were irradiated with UV light to induce the ejection of photo-electrons from the film surface, which were subsequently collected by an air-filled counter with a resolution of ±0.02 eV. Fig. 5 shows a plot of the cube root of the photoelectron emission intensity varying with energy [18]. The work function was obtained from the lower energy threshold of photoemission: 5.25 eV for the 43-nm thick film, 5.20 eV for the 90-nm thick film, 5.08 eV for the 129-nm thick film, and 5.12 eV for the 183-nm thick film. Taking into account the error due to surface contamination, the work function appeared to decrease generally with increasing film thickness. Since the photo-electrons were excited from a depth of 1 nm [19], the differences in film thickness should not have affected the work function. Instead, this trend in the work function suggested that the electron density distribution at the film surface must have increased with increasing film thickness, consistent with the carrier concentrations measured using the Hall Effect (see Table 2).

Table 2
Results of Hall effect measurements on dc magnetron-sputtered ZITO films: comparing film thickness, carrier concentration, and absorption onset

Film thickness [nm]	Carrier concentration [$\times10^{20}$ cm^{-3}]	Absorption onset [eV]
43	1.75	3.74
90	1.89	3.65
129	2.10	3.6
183	1.93	3.52

A more technologically compelling aspect of these results was that all work function values were above 5.0 eV, *i.e.* closer to the typical values for the highest occupied molecular orbital (HOMO) level in organic electroluminescent semiconductors [20,21]. The work function of an ITO film was measured to be 4.63 eV, while that of an IZO film was 5.15 eV. The ZITO thin films are therefore more advantageous for electrode applications requiring a lower hole-injection barrier into the organic layer HOMO levels in contrast to ITO, while performing comparably to IZO (Fig. 6).

Transmittance, reflectance and the surface work function were characterized for ZITO films deposited from the 1:2:1 target. Films of four thicknesses, 43 nm, 90 nm, 129 nm, and 183 nm, were grown on glass coverslip substrates. Transmission and near-normal reflection spectra were obtained using a Shimadzu UV-3150 UV-visible-near IR spectrophotometer with the reflectance accessory and integrating sphere. The thinnest film (43 nm) had the highest transmissivity, ~90% over the

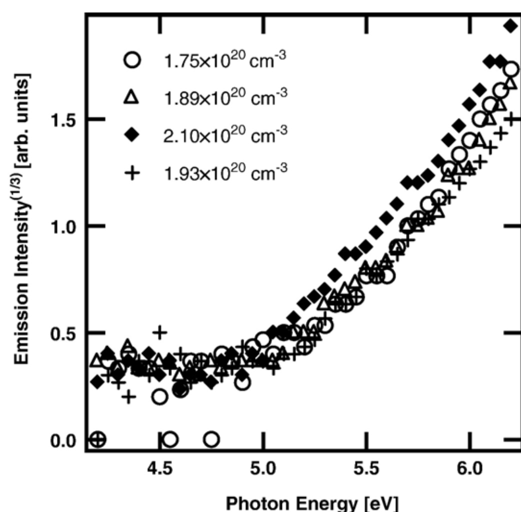

Fig. 5. Plot of the cube root of the photoelectron emission intensity as a function of irradiated photon energy for films of nominal 1:2:1 cation ratio. Carrier concentration is given for the films measured, and the corresponding film thickness can be obtained from Table 2.

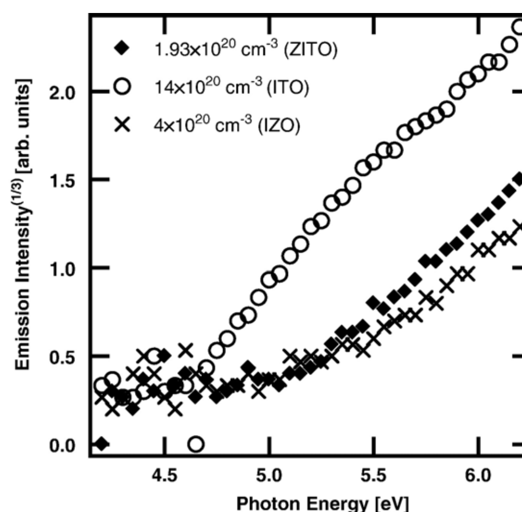

Fig. 6. Plot of the cube root of the photoelectron emission intensity as a function irradiated photon energy, comparing the work function of the 183-nm thick ZITO (1:2:1) film with the work function of a 150-nm thick ITO film and a 200-nm thick IZO film.

Author's personal copy

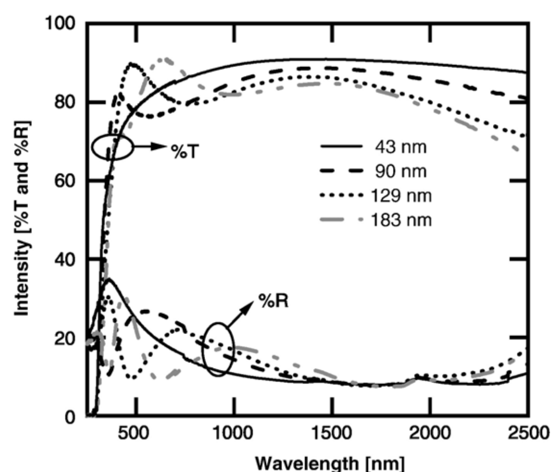

Fig. 7. Transmissivity and near-normal reflectance spectra of ZITO (1:2:1) films of thicknesses 43, 90, 129 and 183 nm.

broadest spectral range, as seen in Fig. 7. From these data, the absorption spectrum for each sample was calculated using

$$T = (1 - R)\exp(-\alpha^{*} d), \quad (1)$$

where d represents the film thickness and α the absorption.

To extract the onset of optically induced electronic transitions for each sample, we used the Tauc equation [22], plotting $(\alpha h\nu)^{1/2}$ as a function of $h\nu$, and extrapolated the linear regions of the absorption spectra to zero absorption ($\alpha h\nu = 0$), as shown in Fig. 8:

$$\alpha h\nu \sim (h\nu - E_g)^2. \quad (2)$$

In *crystalline* semiconductors, α scales with $(h\nu - E_g)^n$, where $n = 2$ for indirect gap (single electron, single phonon, plus a single photon) and $n = 1/2$ for direct gap (single electron plus a single photon) transitions, ignoring excitonic effects. Such a model can be applicable to amorphous materials to a limited extent, due to the lack of long-range order. By adding perturbations to the perfect crystalline lattice, the density of states for the valence band and conduction band could be modeled for an amorphous solid, and the results were supported by empirical observations. However, in amorphous semiconductors, one must also take into account the fact that electron wavefunctions are localized due to the lack of long-range order. Only energy is conserved during an interband transition, while momentum is not. The Tauc equation could therefore only be used to extrapolate the onset of interband transitions, omitting details about the type of interband transition [23]. The extrapolation yielded absorption onset values ranging from 3.52 to 3.74 eV.

Interestingly, because film thickness correlated with an increase in the carrier concentration, Fig. 9 reveals an anomalous narrowing of the band gap with increasing charge carrier density. According to Burstein–Moss theory [24], a degenerately doped semiconductor with a doping level exceeding the Mott critical density should show the opposite behavior. The lowest lying states in the conduction band would be completely filled, resulting in the lowest available unoccupied state to have an energy higher than the conduction band edge. Thus, the measured interband transition energy would be larger than the true gap value. To estimate the Mott critical density, n_c, for doped In_2O_3 films, the following equation [25] was used

$$n_c^{1/3} \approx 0.25\left(\frac{\pi e^2 m_c^{*}}{h^2 \varepsilon_0 \varepsilon^M}\right), \quad (3)$$

where m_c^{*} is the conduction band effective mass and ε^M is the static dielectric constant of the host lattice. For In_2O_3, $m_c^{*} = 0.35\,m$, where m is the free electron mass, and $\varepsilon^M = 8.9$, yielding $n_c \approx 6 \times 10^{18}$ cm^{-3} [26]. Due to the extremely high doping level in

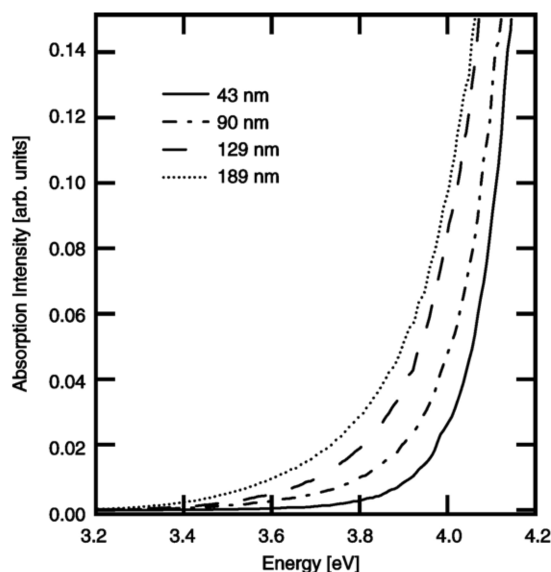

Fig. 8. Absorption spectra for the films in Fig. 7.

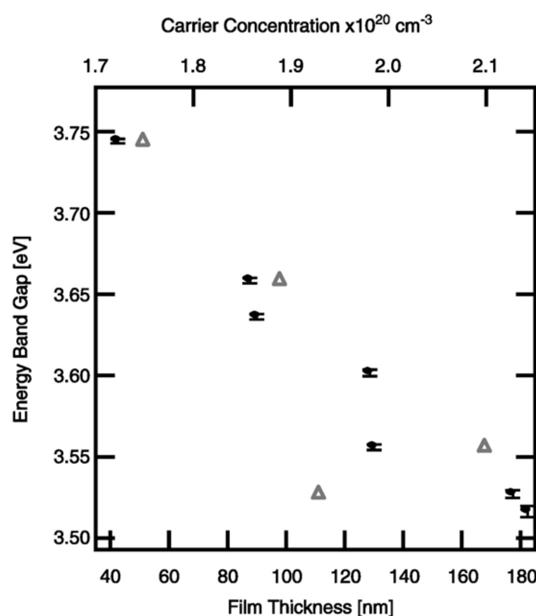

Fig. 9. The forbidden energy gap was observed to decrease with increasing film thickness (*i.e.*, black filled circles with error bars) and increasing carrier concentration (*i.e.*, gray open triangles), as measured by Hall Effect.

Author's personal copy

the nominally 1:2:1 films, the m_c^* and ε^M values of In_2O_3 might differ but not so much as to shift the critical density by more than an order of magnitude, so the films characterized could all be consider heavily doped, and a Burstein–Moss shift should be apparent. Mechanisms for a possible narrowing of the measured band gap have been proposed [27–29], but the widening effect of the Burstein–Moss shift should still dominate over gap-narrowing effects due to many body interactions, donor impurity structural arrangement and disorder in the atomic arrangement [26,30]. While the reason for the anomalous band gap narrowing with increasing carrier density is still being considered, the range of extracted band gap values for the ZITO films, 3.52–3.74 eV, nevertheless offers a broader transmission window for visible light than that of IZO (2.9 eV [7]) and coincides with that of ITO, 3.5–4.3 eV [26].

4. Conclusions

Thin films of amorphous ZITO of cation ratios 1:2:1 and 1:2:1.5 were grown by dc magnetron sputtering from a multi-phase vacuum hot-pressed target. Substrates pre-heated to 300 °C yielded films with better electrical properties than unheated substrates, and the incorporation of oxygen to 0.4 vol.% was necessary only in the 1:2:1.5 films to optimize the electrical performance. Optical transmissivity of all films was >80% of visible light. Although the lowest electrical resistance of 7.6×10^{-4} Ω-cm is slightly higher than that of *a*-IZO, 3–6×10^{-4} Ω-cm, as well as that of *a*-ITO, 1–2×10^{-4} Ω-cm, ZITO thin films are suitable alternatives to *a*-ITO owing to deposition from lower-cost sputter targets and an increased stability of the amorphous microstructure, which enables more uniform etch rates. Moreover, the work function being greater than 5.0 eV renders ZITO to be a more efficient hole-injection electrode in organic light emitting diodes, and the exact value can be tuned by adjusting the ratio of relative cation content.

Acknowledgements

The authors would like to thank Dr. Yasushi Sato of Aoyama Gaukin University for work function measurements.

References

[1] T. Minami, MRS Bull. 25 (2000) 38.
[2] M.P. Taylor, D.W. Readey, C.W. Teplin, M.F. van Hest, J.L. Alleman, M.S. Dabney, L.M. Gedvilas, B.M. Keyes, B. To, P.A. Parilla, J.D. Perkins, D.S. Ginley, Macromol. Rapid Commun. 25 (2004) 3444.
[3] B. Yaglioglu, H.Y. Yeom, D.C. Paine, Appl. Phys. Lett. 87 (2005) 1.
[4] C.W. Ow-Yang, D. Spinner, Y. Shigesato, D.C. Paine, J. Appl. Phys. 83 (1998) 145.
[5] G.B. Palmer, K.R. Poeppelmeier, T.O. Mason, Chem. Mater. 9 (1997) 3121.
[6] J.M. Phillips, R.J. Cava, G.A. Thomas, S.A. Carter, J. Kwo, T. Siegrist, J.J. Krajewski, J.H. Marshall, W.F. Peck Jr., D.H. Rapkine, Appl. Phys. Lett. 67 (1995) 2246.
[7] T. Minami, J. Vac. Sci. Technol. 17 (1999) 1765.
[8] A.J. Freeman, K.R. Poeppelmeier, T.O. Mason, R.P.H. Chang, T.J. Marks, MRS Bull. 25 (2000) 45.
[9] C.W. Ow-Yang, H.-Y. Yeom, B. Yaglioglu, D.C. Paine, in: H. Ohta, et al., (Eds.), Materials for Transparent Electronics, Boston, MA, U.S.A., November 28–December 2, 2005, Materials Research Society Symposium Proceedings, vol. 905E, 2005, 0905-DD01-07.
[10] H.Y. Yeom, N.D. Popovich, E. Chason, D.C. Paine, Thin Solid Films 411 (2002) 17.
[11] Y. Sato, R. Tokumaru, E. Nishimura, P.-K. Song, Y. Shigesato, K. Utsumi, H. Iigusa, J. Vac. Sci. Technol. 23 (2005) 1167.
[12] G. Frank, H. Köstlin, Appl. Phys., A 27 (1982) 197.
[13] G. Gonzalez, J. Cohen, J. Hwang, T.O. Mason, J.P. Hodges, J.D. Jorgenson, J. Appl. Phys. 89 (2001) 2550.
[14] Y. Shigesato, D.C. Paine, Appl. Phys. Lett. 62 (1993) 1268.
[15] B. Yaglioglu, Y.-J. Huang, H.Y. Yeom, D.C. Paine, Thin Solid Films 496 (2006) 89.
[16] Y.-S. Jung, J.-Y. Seo, D.-W. Lee, D.-Y. Jeon, Thin Solid Films 445 (2003) 63.
[17] J.D. Bellingham, W.A. Phillips, C.J. Adkins, J. Phys., Condens. Matter 2 (1990) 6207.
[18] P.E. Carroll, Phys. Rev. 104 (1956) 660.
[19] H. Ago, T. Kugler, F. Cacialli, W.R. Salaneck, M.S.P. Shaffer, A.H. Windle, R.H. Friend, J. Phys. Chem., B 103 (1999) 8116.
[20] J.S. Kim, B. Laegel, E. Moons, N. Johansson, I.D. Baikie, W.R. Salaneck, R.H. Friend, F. Cacialli, Synth. Met. 111–112 (2000) 311.
[21] T.M. Brown, F. Cacialli, J. Polym. Sci., B, Polym. Phys. 41 (2003) 2649.
[22] J. Tauc, R. Grigorovici, A. Vancu, Phys. Status Solidi 15 (1966) 627.
[23] J. Tauc, in: F. Abeles (Ed.), Optical Properties of Solids, North-Holland Publishing, Amsterdam, 1972, p. 279.
[24] E. Burstein, Phys. Rev. 93 (1953) 632.
[25] N.F. Mott, Metal-Insulator Transitions, Taylor-Francis, London, 1974.
[26] I. Hamberg, C.G. Granqvist, J. Appl. Phys. 60 (1986) R123.
[27] N.F. Mott, J. Phys. C. Solid State Phys. 13 (1980) 5433.
[28] S.K. O'Leary, Solid State Commun. 109 (1999) 589.
[29] B.E. Sernelius, K.-F. Berggren, Z.-C. Jin, I. Hamberg, C.G. Granqvist, Phys. Rev., B 37 (1998) 10244.
[30] A.P. Roth, J.B. Webb, D.F. Williams, Phys. Rev., B 25 (1982) 7836.
[31] Powder Diffraction File, Joint Committee on Powder Diffraction Standards, ASTM, Philadelphia, PA, 2001, Cards 06-0416, 74-2184, 79-0205, 88-0773, 77–0191.